Journal of Superconductivity, Vol. 7, No. 6, 1994

Review

Thermal and Nonequilibrium Responses of Superconductors for Radiation Detectors

Z. M. Zhang[1] and A. Frenkel[1]

Received 3 January 1994

This work summarizes the progress in the study of the superconductor response to optical radiation and in the development of infrared detectors. The recent advances in the design of high-T_c superconducting radiation detectors using silicon microfabrication technology are emphasized. Thermal and optical properties important for the detector performance are discussed. The mechanism of the nonequilibrium optical response and its potential use to build fast and sensitive radiation detectors are described. Future challenges and opportunities in the development of high-T_c superconducting radiation detectors are highlighted.

KEY WORDS: Superconducting radiation detectors; photoresponse; nonequilibrium optical response; optical properties; thermal design.

1. INTRODUCTION

One of the most promising applications of superconducting materials is the construction of highly sensitive optical radiation detectors. Such detectors have many applications, including space radiometry for earth and planetary observations, optical communication, thermal imaging for military and biomedical applications, spectroscopy, and pyrometry or noncontact temperature measurements. High-T_c superconducting detectors are potentially the most sensitive radiation detectors operated at temperatures above 77 K for radiation at wavelengths longer than 20 μm [1]. Figure 1 is a schematic of a superconducting radiation detector. A bias current is applied to a superconducting film, and a voltmeter measures the voltage across the film. The voltage signal induced by the incident radiation is called optical response or photoresponse. Optical response of superconductors can be divided into two categories. One is the thermal, or bolometric, response, which is due to a temperature change caused by the heating effect of the incident radiation. This temperature change introduces a measurable change in some physical properties, for example, the electrical resistance of a superconductive material in the superconducting-to-normal state transition. The other is the nonequilibrium, or nonbolometric, response, which occurs at temperatures below the transition. In this case, the incident photons break the superconducting electron pairs, the Cooper pairs, and cause an increase in the number density of quasiparticles. The nonequilibrium response may happen on a time scale comparable to or less than the electron–phonon relaxation time and, in principle, can be used to build fast and sensitive radiation detectors.

Clarke *et al.* [2] reviewed the development of low-T_c superconducting bolometers. Kruse [3], Frenkel [4], and Khrebtov [5] discussed the thermal and nonequilibrium detectors using both low-T_c and high-T_c superconducting materials. The objective of this paper is to discuss the latest progress in the study of optical response of superconductors and further research needed for the development of superconducting radiation detectors.

In addition to the resistive bolometer, other thermal detectors, such as the kinetic-inductance superconducting radiometer, high-T_c superconducting

[1]Radiometric Physics Division, National Institute of Standards and Technology, Gaithersburg, Maryland 20899.

0896-1107/94/1200-0871$07.00/0

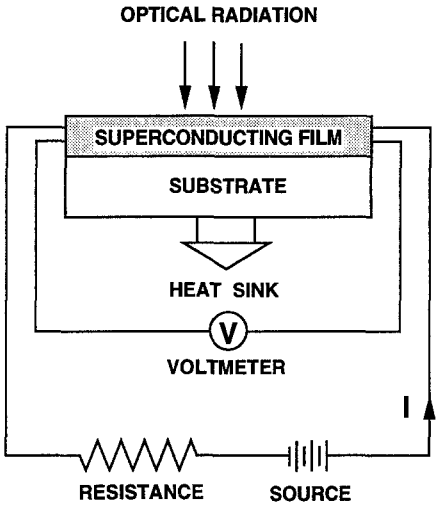

Fig. 1. Schematic of a superconducting radiation detector.

magnetic-susceptibility bolometer, and the intrinsic superconducting radiation detector, were proposed [6–9]. Fast bolometric response with response time on the nanosecond scale was observed [10, 11]. Silicon microfabrication technology has created opportunities for the semiconductor–superconductor hybrid electronics, which has great potential for detector-array applications [12, 13].

Nonequilibrium optical response has been observed for low-T_c and more recently for high-T_c superconductors. A recent analysis of the mechanism of optical response of high-T_c superconductors suggested that, with proper optimization of device parameters, fast and sensitive detectors covering a broad electromagnetic spectrum could be developed [14].

There are many opportunities and challenges in the research of thermal and nonequilibrium responses of superconductors and in the development of superconducting radiation detectors. Thermal modeling and design are required to predict the dynamic response of superconducting infrared detectors. In order to perform a thermal design, it is necessary to determine the thermophysical properties, such as the absorptance and thermal conductivity of the superconducting films and substrates at operating temperatures. The boundary resistance between the superconducting film and the substrate is also important for the prediction of the detector performance. Since the detector will operate at cryogenic temperatures, cooling and temperature control techniques are essential to achieve the required temperature stability. Improving microfabrication and patterning techniques will improve the performance of detector arrays using superconducting films on silicon substrates. Further theoretical and experimental investigations on the nonequilibrium response mechanism are required for the realization of radiation detectors sensitive in a broad electromagnetic spectrum with a response time of the order of picoseconds.

2. THERMAL DETECTORS

2.1. Superconducting Bolometers

A bolometer measures the incident radiation by detecting a change in the electrical resistance resulting from a temperature change due to the heating effect of the incident radiation. As shown in Fig. 1, modulated or pulsed radiation is incident on a superconducting film, causing the temperature of the film–substrate composite to vary relative to that of a temperature-stabilized heat sink. A constant bias current is applied and a voltmeter measures the voltage across the superconducting film. A superconducting bolometer employs the strong temperature dependence of the electrical resistance in the transition region near T_c. Figure 2 illustrates the operating mechanism of a superconducting bolometer, where the voltage response is proportional to the temperature derivative of the electrical resistance. Ohm's law gives the change of the voltage across the superconducting film as

$$\Delta V = I\frac{dR}{dT}\Delta T \tag{1}$$

where I is the bias current, R is the electrical resistance of the superconductor, and ΔT is the temperature difference between the film–substrate composite and the heat sink.

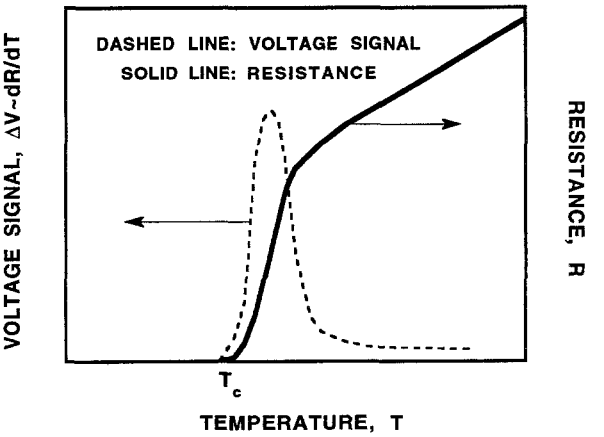

Fig. 2. Operating mechanism of a superconducting bolometer.

The heat transfer process in a detector system is often simplified with a lumped parameter model, i.e., a heat capacity C connected to a heat sink through a thermal conductance G. Both parameters may depend on the modulation frequency. For incident radiation with radiant power P and modulated at an angular frequency ω_m, the transient heat conduction equation is [15,16]

$$C\frac{d\Delta T}{dt}+G\Delta T=I^2R+\alpha P(1+\cos\omega_m t) \qquad (2)$$

where α is the absorptance of the detector and I^2R is the Joule heating power. A first-order expansion of the electrical resistance at temperatures near the heat-sink temperature, T_0, is $R=R_0+(dR/dT)\Delta T$, where R_0 and dR/dT are the electrical resistance and its temperature derivative at T_0. A steady-state solution of Eq. (2) gives

$$\Delta T=\frac{\alpha P\cos(\omega_m t-\tan^{-1}\omega_m\tau)}{G_{eff}(1+\omega_m^2\tau^2)^{1/2}}+\frac{\alpha P+I^2R_0}{G_{eff}} \qquad (3)$$

where $\tau=C/G_{eff}$ is the thermal time constant of the detector and $G_{eff}=G-I^2(dR/dT)$ is the effective thermal conductance. Since $dR/dT>0$, the requirement of positive G_{eff} sets a stability criterion which limits the bias current [2]. The last term in Eq. (3) does not depend on time and is often dropped since for many applications only the temperature change with time needs to be considered. This term determines the average temperature of the detector and, therefore, is important for thermal modeling and design. It is also necessary to include this term in some applications, such as absolute radiometers.

The responsivity S of a radiation detector is the ratio of the output voltage amplitude to the incident power amplitude. From Eq. (1) and Eq. (3), one obtains

$$S=\frac{\alpha I(dR/dT)}{G_{eff}(1+\omega_m^2\tau^2)^{1/2}} \qquad (4)$$

The ultimate sensitivity of a radiation detector is determined by the noise equivalent power, *NEP*. The square of the *NEP* of a bolometer can be written as [1,2,17,18]

$$NEP^2=\frac{8\sigma_{S\text{-}B}k_BAT_b^5}{\alpha}+\frac{4k_BT^2G}{\alpha^2}+\frac{4k_BTR}{S^2}+\frac{4k_BT_aR_a}{S^2}+\frac{\gamma I^2R_0^2}{\omega_m S^2} \qquad (5)$$

The first term is the background noise, calculated for a hemispherical blackbody source in the whole spectrum, where k_B is the Boltzmann constant, $\sigma_{S\text{-}B}$ is the Stefan–Boltzmann constant, T_b is the background temperature, and A is the detector receiving area. The second term is the phonon noise caused by the random exchange of energy between the detector element and the heat sink through the thermal conductance. The third and fourth terms are the Johnson noises of the bolometer and the amplifier, respectively, where R_a and T_a are the resistance and operating temperature of the amplifier. The Johnson noise is associated with the thermal fluctuation in a resistive element. The last term is the $1/f$ noise, where γ is a constant.

Another figure of merit of a detector is the detectivity, D^*, which is defined as

$$D^*=A^{1/2}/NEP \qquad (6)$$

An increase of the detector absorptance yields an increase of the responsivity and D^* and a decrease of the *NEP*. It is also desirable to reduce the heat capacity to achieve fast response. A coating could be used to increase the absorptance which would cause an increase in the response time. Without a coating, the absorptance depends on the thicknesses of the superconducting film and the wavelength of the incident radiation, which will be discussed in more detail in Section 4.1. A decrease of the thermal conductance improves the responsivity and *NEP* but degrades the dynamic range and time response. High-quality epitaxial films exhibit a sharp transition which improves the responsivity. The excess $1/f$ noise in a superconducting film can be reduced by improving the film quality [19].

Brasunas and Lakew [20] constructed a composite high-T_c superconducting bolometer using an $YBa_2Cu_3O_7$ film on a mechanically polished $LaAlO_3$ substrate with a thickness of 75 μm. The time constant of this bolometer was 150 ms and D^* was 1.5×10^6 m $Hz^{1/2}$ W^{-1} at 5 Hz. Verghese *et al.* [21] fabricated a superconducting bolometer with an *NEP* of 2.4×10^{-11} W $Hz^{-1/2}$ at 10 Hz and a time constant of 55 ms. An epitaxial $YBa_2Cu_3O_7$ superconducting film was deposited on a sapphire substrate with a $SrTiO_3$ buffer layer. The substrate was lapped to 20 μm after deposition to reduce the heat capacity. Spectral measurements using a Fourier-transform spectrometer showed that this bolometer has useful sensitivity from visible to beyond 100 μm [21].

Fast bolometric response of the order of nanosecond has been observed by several research groups using pulsed laser and synchrotron radiation sources from the visible to the far-infrared [10,11,22–25]. This

can be understood by considering the thermal coupling between the superconducting film and the substrate. During the first few nanoseconds when the pulsed radiation is absorbed by the film, the film temperature increases relative to the substrate. The time constant is equal to the heat capacity of the film divided by the thermal conductance between the film and the substrate. A slower tail always accompanies the fast response due to the heating of the substrate.

Another possible explanation of the fast bolometric response results from consideration of the heat transfer into the substrate using a one-dimensional heat transfer model [25]. In this model, the thickness and heat capacity of the film and the boundary resistance between the film and the substrate were neglected. The optical pulse was simplified as a step heating source at the surface of the substrate with a duration equal to the full width at half maximum (FWHM) of the pulse. A decay time of 3 ns was predicted for a 150 ps pulse [25].

The importance of the thermal coupling between the film and the substrate was also demonstrated by Dwir and Pavuna [24]. They patterned a $20 \times 20\ \mu m^2$ $YBa_2Cu_3O_7$ microbridge and a meander line structure on $SrTiO_3$ substrates. The spectral response of both devices was tested from the visible to 450 μm.The detector with the meander line showed a higher responsivity, which was 800 V W^{-1}, while that with the microbridge showed useful responses for chopping frequencies at more than 10 kHz [24].

2.2. Superconducting Microbolometers and Detector Arrays

Antenna-coupled high-T_c superconducting microbolometers were analyzed by Hu and Richards [26]. These detectors are designed for the far-infrared and microwave applications. Nahum *et al.* [23] fabricated a microbolometer using an $YBa_2Cu_3O_7$ film with an area of $6 \times 13\ \mu m^2$ on an yttria-stabilized zirconia (YSZ) substrate. The electrical *NEP* was 4.5×10^{-12} W $Hz^{-1/2}$ measured at a modulation frequency of 10 kHz. The main drawback of this microbolometer was that the optical efficiency was only 5%. Li *et al.* [27] tested $YBa_2Cu_3O_7$ microbolometers fabricated on YSZ substrates using chopped argon-ion laser at wavelength of 0.514 μm as the radiation source. They obtained a responsivity of $\sim$1000 V W^{-1} at a chopping frequency of 100 Hz for a $2.5 \times 2.5\ \mu m^2$ film. The response time decreased from 40 to 5 μs when the chopping frequency was increased from 100 to 4000 Hz.

Perhaps the most prominent progress in the advance of superconducting bolometers is the microfabricated high-T_c bolometers on silicon or silicon nitride substrates, since these structures have potential for infrared imaging arrays and are ideal for integrated semiconductor–superconductor electronics. Stratton *et al.* [28] designed and constructed such a superconducting microbolometer. A 400-nm-thick Si_3N_4 membrane was deposited on a Si substrate, and the center part of the Si substrate was then removed by chemical etching. This process left a Si_3N_4 membrane suspended on a Si substrate. The YSZ buffer layer and $DyBa_2Cu_3O_7$ film were deposited on the Si_3N_4 membrane. The thickness of the superconducting film was 300 nm and that of the YSZ buffer layer was 60 nm. The lateral dimensions of the superconducting film was $75 \times 75\ \mu m^2$. This structure resulted in a small heat capacity and a good thermal isolation. A responsivity of 800 V W^{-1} and a time constant of 1 ms were obtained [28]. Johnson *et al.* [13] reported superconducting $YBa_2Cu_3O_7$ detector arrays fabricated by silicon micromachining. A linear detector array containing 12 pixels was formed on a 300-nm-thick Si_3N_4 membrane. Each pixel was 1.05 μm thick with an area of $85 \times 115\ \mu m^2$. The $YBa_2Cu_3O_7$ meander line was patterned on each pixel 4 μm wide and approximately 1.1 mm long. The thermal conductance between the detector element and the substrate at temperatures from 70 to 90 K was determined to be from 2×10^{-7} to 3×10^{-7} W K^{-1} due to the low thermal conductivity of the Si_3N_4 membrane, and the time constant was 24 ms. They also found that the noise in the microbolometers was dominated by the noise in the $Au/YBa_2Cu_3O_7$ contacts. If the contact noise could be eliminated, the *NEP* would be reduced to the calculated *NEP* of 9×10^{-13} W $Hz^{-1/2}$. These results make the high-T_c microbolometers comparable with the HgCdTe staring focal plane arrays. Moreover, silicon-microfabricated superconducting bolometers are cost effective, sensitive to longer wavelengths, and feasible for on-chip read-out electronics.

Verghese *et al.* [12] investigated the feasibility of using high-T_c superconducting bolometers to form infrared imaging arrays. They pointed out that the film quality strongly affects the detector performance. Epitaxial films exhibit a sharp transition, which improves the responsivity, and low $1/f$ noise. Considering the fact that superconducting films deposited on silicon nitride are not epitaxial and have a wide transition, Fenner *et al.* [29] and Li *et al.* [30] fabricated epitaxial $YBa_2Cu_3O_7$ superconducting bolometers on thin silicon wafers. The thickness of the wafers

ranged from 400 μm down to 4 μm. Epitaxial $YBa_2Cu_3O_7$ films were deposited on these substrates with YSZ buffer layers by pulsed laser ablation. The zero-resistance critical temperature of these films ranged from 83 to 89 K with transition widths less than 2 K. A responsivity of 1750 V W^{-1} was demonstrated for a film on a 25-μm-thick Si wafer. The rise time was 3 ms for a film on a 4-μm-thick Si wafer. The lowest *NEP* observed was 7×10^{-10} W $Hz^{-1/2}$ at 10 Hz for the film on the 25-μm-thick Si wafer, which was limited by the amplifier noise. YBCO and YSZ films were also deposited on a 0.75-μm-thick silicon window micromachined into a 400-μm-thick wafer. A rise time of 500 μs was achieved with this device (30).

Bang *et al.* [31, 32] presented a novel microfabricated superconducting detector, which combined small heat capacity and excellent thermal isolation with high film quality. A single-crystal Si island was formed on a Si_3N_4 membrane using a wafer bonding technique. The single-crystal silicon served as the substrate for the superconducting film, and the Si_3N_4 membrane thermally isolated the detector-sensing element from the substrate. Figure 3 shows the structure of the microfabricated superconducting detector, where the thickness of the Si island is approximately 0.25 μm. The predicted time constant and *NEP* were less than 200 μs and 2.0×10^{-12} W $Hz^{-1/2}$,

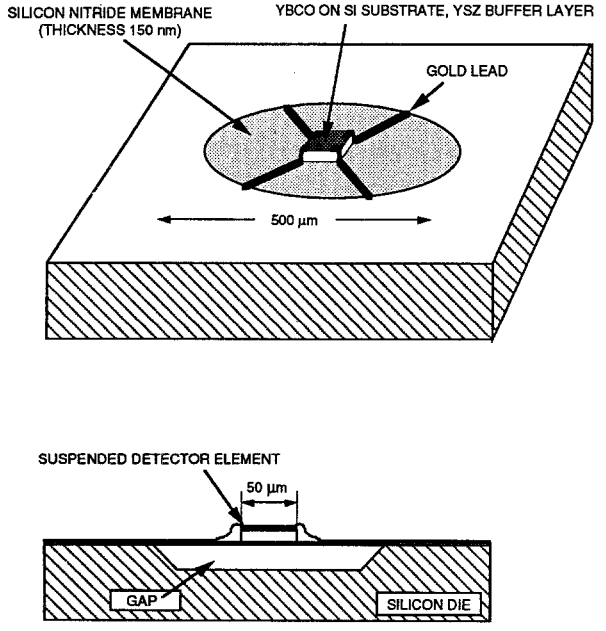

Fig. 3. Microfabricated superconducting detector (from [32] by permission of the author).

respectively. Polycrystalline YBCO films with sharp resistance transition at ~90 K were deposited on this structure. Epitaxial films could be deposited by removing the native oxide on the silicon and improving processing control [32]. Further studies are required to realize the potential use as detector arrays and to develop on-chip integrated read-out electronics.

2.3. Superconducting Kinetic-Inductance Radiometer

McDonald [7] proposed a superconducting kinetic-inductance thermometer based on the temperature dependence of the magnetic penetration depth. It works below the critical temperature and eliminates the Johnson noise in the superconducting bridge. It is also compatible with a very low noise SQUID (superconducting quantum interference device) amplifier. A superconducting kinetic-inductance radiometer is being developed for the absolute spectral irradiance measurement [6]. The mechanism of the superconducting kinetic-inductance thermometer is illustrated in Fig. 4. The penetration depth of the superconducting film is monitored through the inductance of the microstripline. In the kinetic inductance limit, the magnetic penetration depth of the film, λ, is much larger than the film thickness, d_f. The contribution of the superconducting film to the kinetic inductance of the microstripline was given as [7]

$$L = \mu_0 \frac{l}{w} \frac{\lambda^2}{d_f} \tag{7}$$

where μ_0 is the magnetic permeability of free space, and l and w are the length and width of the microstripline, respectively. Based on the two-fluid model, the penetration depth is [33]

$$\lambda(T) = \left(\frac{m_e}{\mu_0 e^2 n_s(T)} \right)^{1/2} \tag{8}$$

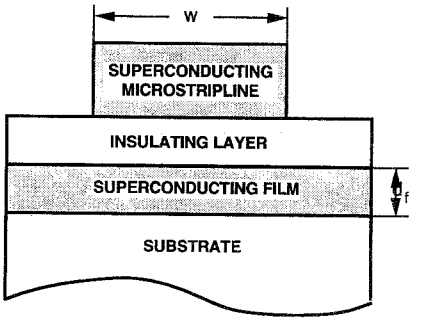

Fig. 4. Illustration of the superconducting kinetic-inductance thermometer.

where e and m_e are the electron charge and effective mass, and n_s is the number density of the superconducting electrons, which is related to temperature and the total electron number density n_e by

$$n_s(T)=n_e[1-(T/T_c)^4] \tag{9}$$

Equations (7), (8), and (9) describe the temperature-dependent kinetic inductance of a superconducting film. The nonequilibrium effect on the kinetic inductance caused by the direct reduction of the number density of superconducting electrons by the incident photons will be discussed in the section on the nonequilibrium response.

An *NEP* of 0.7×10^{-12} W for a 100 s integration time was measured for a prototype thermometer operated from 4 to 8 K using niobium superconducting film and microstripline [6]. Since high-T_c superconductors have a larger penetration depth than low-T_c superconductors, there is a potential for constructing radiation detectors based on the kinetic inductance of high-T_c superconducting films.

2.4. High-T_c Superconducting Magnetic-Susceptibility Bolometer

Brasunas *et al.* [8] proposed a superconducting bolometer based on the temperature dependence of the diamagnetic screen caused by a superconducting film. As shown in Fig. 5, the high-T_c superconducting film is suspended inside a copper coil by a silicon rod. The temperature change due to the incident radiation alters the diamagnetic screening of the high-T_c superconducting film. A change in the diamagnetism or ac susceptibility causes a change in the self-inductance of the coil. If an ac bias current I is applied at a frequency f, the change in the voltage of the coil is given by

$$\Delta V=2\pi fI\Delta L \tag{10}$$

where ΔL is the change of the self-inductance of the coil, which depends on the temperature change ΔT in the superconducting state. The temperature dependence of ΔL is large at temperatures close to but less than T_c. The advantage of this detector is that there is no transport current through the superconducting film. A device with a predicted *NEP* of 10^{-11} W $Hz^{-1/2}$ using a high-T_c $YBa_2Cu_3O_7$ film was described in [8].

2.5. Intrinsic Superconducting Radiation Detector

The critical current of a superconducting film is a function of temperature and can be employed to determine the radiant power [9,34,35]. Since the detector is based on the temperature dependence of the critical current and operates just below the critical current for a given temperature, it was called the intrinsic superconducting radiation detector (ISRD). Figure 6 shows the operating points of the ISRD. The bias current is increased until the voltage across the superconducting bridge exceeds a voltage threshold, V_c, defining the critical current which is a function of the temperature of the superconducting bridge. The Johnson noise and Joule heating are negligible in the superconducting bridge. The responsivity (in A W^{-1}) of the ISRD is proportional to the temperature derivative of the critical current [9]:

$$S=\frac{\alpha}{G}\left|\frac{dI_c}{d\Delta T}\right| \tag{11}$$

Flik *et al.* [9] showed that an *NEP* of 2.6×10^{-12} W Hz^{-12} and D^* of 2.7×10^7 m $Hz^{1/2}$ W^{-1} could be achieved using an $YBa_2Cu_3O_7$ film. For the

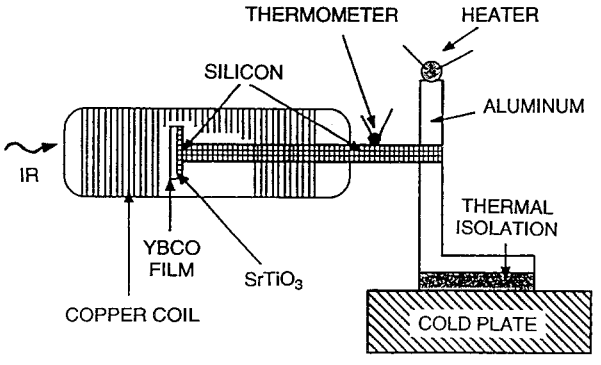

Fig. 5. High-T_c superconducting magnetic-susceptibility detector (from [8] by permission of the author).

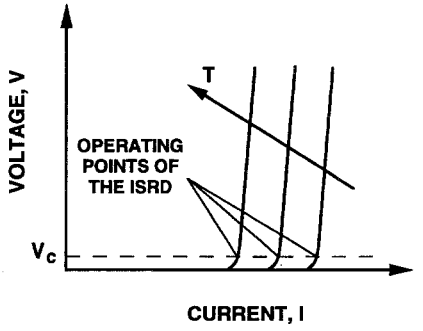

Fig. 6. Operating point of the intrinsic superconducting radiation detector (from [9]).

practical realization of the ISRD, further investigations are required on the $1/f$ noise for currents just above the critical current, the accuracy of the critical current measurement using a ramp technique, and the possible existence of hysteresis due to the magnetic flux motion [9].

3. NONEQUILIBRIUM RESPONSE

Gilabert [36], Kruse [3], and Frenkel [4] summarized earlier studies of nonequilibrium response of superconductors. The nonequilibrium response for low-T_c superconducting films is due to the generation of quasiparticles which, in turn, may cause a suppression of the superconducting energy gap as reviewed in [37–39]. The observed nonequilibrium response for granular films was attributed to the Josephson junction or weak link at grain boundaries [40–42]. Low-T_c superconductor Josephson junction detectors, employing either a bolometric or a nonbolometric mechanism, hold promise for highly sensitive detectors and detector arrays [2,43–45].

Nonbolometric response in epitaxial films was reported by many research groups [46–54]. Nonbolometric response can happen in a very short time and at temperatures much less than the transition temperature. Moreover, the magnitude of the nonequilibrium response is not proportional to dR/dT. Femtosecond optical study of high-T_c superconducting films using pump and probe techniques resolved an avalanche multiplication process of quasiparticles following photon absorption [55–57]. This process is attributed to inelastic electron–electron scattering on a time scale, $\tau_{e\text{-}e}$, comparable or less than 1 ps. The quasiparticles also interact with phonons through inelastic electron–phonon scattering. The dissipation mechanism could be due to the suppression of energy gap like that in the low-T_c superconductors or due to the vortex motion. The photon-induced reduction of the superconducting electron number density may also cause a change in the kinetic inductance, which can be used to study the nonequilibrium dynamics [53–54] and to build sensitive radiation detectors [58].

Figure 7 illustrates the nonequilibrium interactions among photons, Cooper pairs, quasiparticles, phonons, and vortices. A detailed diagram of interaction was presented in [14]. These processes are explained as follows: (1) Photons interact with Cooper pairs and quasiparticles, creating more high-energy quasiparticles. The photon–electron interaction happens in less than 1 fs [54]. (2) High-energy quasiparticles continuously break Cooper pairs and

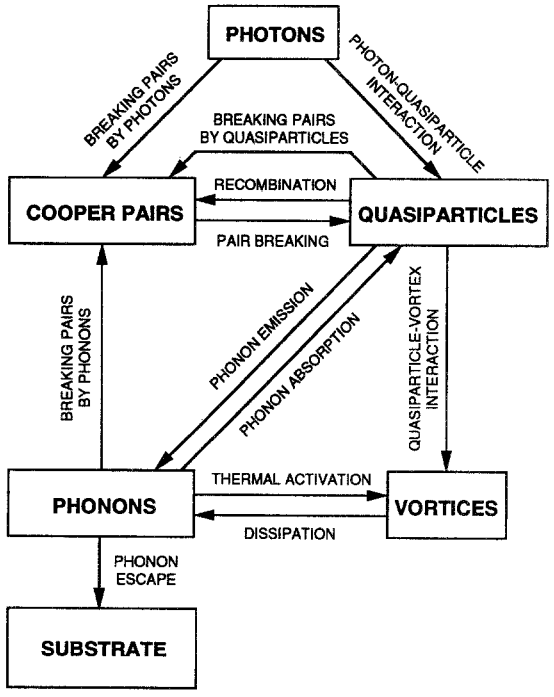

Fig. 7. Nonequilibrium interactions in a superconducting film.

create more quasiparticles on a time scale of $\tau_{e\text{-}e}$. (3) Quasiparticles interact with phonons through phonon emission and absorption ($\tau_{e\text{-}ph}$). (4) High-energy phonons break Cooper pairs (τ_B). (5) Quasiparticles recombine to form Cooper pairs and create phonons (τ_R). (6) Quasiparticles and phonons activate vortex motion, which causes dissipation. The time scales are $\tau_{e\text{-}v}$, $\tau_{ph\text{-}v}$, and τ_d. (7) Phonons escape from the film to the substrate on a time scale, τ_{es}, typically a few nanoseconds.

Following the work of Anisimov *et al.* [59] and Qiu and Tien [60] for the interaction of short laser pulse with metals, the electron and phonon systems may be considered in thermodynamic equilibrium with themselves. The effective electron and phonon temperatures in a superconductor are described by [14]

$$C_e \frac{dT_e}{dt} = k_e \nabla^2 T_e - \gamma_{e\text{-}ph}(T_e - T_{ph}) - \gamma_{e\text{-}v}(T_e - T_0) + q_{ab} \tag{12}$$

$$C_{ph} \frac{dT_{ph}}{dt} = k_{ph} \nabla^2 T_{ph} + \gamma_{e\text{-}ph}(T_e - T_{ph}) - \gamma_{ph\text{-}v}(T_{ph} - T_0) + q_d \tag{13}$$

where T_e and T_{ph} are the effective electron and phonon temperatures, T_0 is the equilibrium temperature

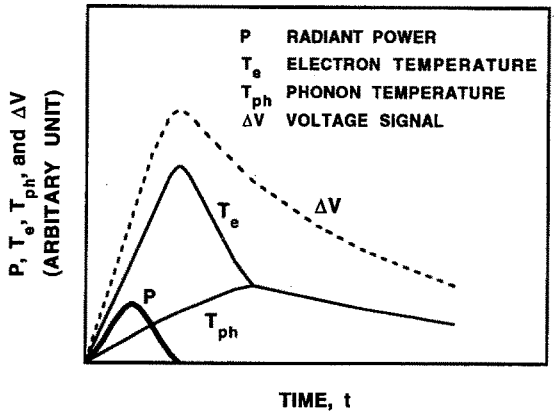

Fig. 8. Time evolution of the radiant power, effective electron and phonon temperatures, and voltage signal (from [14]).

before irradiation, C_e and C_{ph} are the electron and phonon heat capacities per unit volume, k_e and k_{ph} are the electron and phonon thermal conductivities, $\gamma_{e\text{-}ph}$, $\gamma_{e\text{-}v}$, and $\gamma_{ph\text{-}v}$ are the electron–phonon, electron–vortex, and phonon–vortex coupling constants, q_{ab} is the absorbed power density, and q_d is the dissipative power density. The solution of the above coupled equations yields a higher electron temperature compared to the phonon temperature starting from the beginning of the optical excitation. When the time duration is comparable or larger than the electron–phonon relaxation time, the electron temperature will be equalized to the phonon temperature. Figure 8 shows the time evolution of the radiant power, effective electron and phonon temperatures, and voltage signal for pulse duration shorter than the electron–phonon relaxation time [14]. It is assumed that the electron temperature reaches its maximum at the end of the optical pulse and the voltage signal is the largest when the electrons are at the maximum temperature. The phonon escape time is the bottleneck for thermal relaxation. When the pulse duration is much longer than $\tau_{e\text{-}e}$ and $\tau_{e\text{-}ph}$, the effective temperature of electrons may be considered the same as that of phonons.

After the initial avalanche inelastic scattering of quasiparticles by electron–electron and electron–phonon interactions, the rate equations developed by Rothwarf and Taylor [61] can be applied to account for the time dependence of the numbers of quasiparticles and high-energy phonons:

$$\frac{dN_{qp}}{dt} = I_{qp} + \frac{2N_{ph}}{\tau_B} - \frac{N_{qp}^2}{2\tau_R N_{qpT}} \tag{14}$$

$$\frac{dN_{ph}}{dt} = I_{ph} - \frac{N_{ph}}{\tau_B} + \frac{N_{qp}^2}{4\tau_R N_{qpT}} - \frac{N_{ph} - N_{phT}}{\tau_{es}} \tag{15}$$

where N_{qp} and N_{ph} are the numbers of quasiparticles and high-energy phonons with energy greater than the gap energy, 2Δ, N_{qpT} and N_{phT} and their equilibrium values, respectively, and I_{qp} and I_{ph} are the quasiparticle and phonon generation rates due to the external excitation and the electron–phonon interaction. The recombination rate is $(2\tau_R N_{qpT})^{-1}$. The rate equations can be used to estimate the photon-induced change of the superconducting electron number density and, therefore, the change of the energy gap [62].

A response time of less than 120 ps was obtained by Nebosis *et al.* [51] using a 70-nm-thick $YBa_2Cu_3O_7$ stripline detector at temperatures between 78 and 79.5 K. They used an optically pumped far-infrared laser in the wavelength region from 46.5 to 400 μm. The responsivity and *NEP* were 1 mV W^{-1} and 5×10^{-7} W Hz$^{-1/2}$, respectively, which are comparable with other fast far-infrared detectors [51].

Ghis *et al.* [52] recently performed an electrical picosecond measurement of the nonequilibrium response of a *c*-axis-oriented $YBa_2Cu_3O_{7-\delta}$ epitaxial film. They observed a voltage response with a rise time of 12 ps and width of 29 ps across the 30-nm-thick film at 50 K with a bias current of 25 mA. The critical current of this film at 50 K is 40 mA. The radiation source is a 1.5 ps laser pulse at 1.06 μm wavelength with an energy flux of 1 μJ cm^{-2} per pulse.

Frenkel [14] discussed methods to reduce the phonon escape time by eliminating boundary resistance and employing superconducting narrow stripes. The sensitivity of nonequilibrium superconducting detector could be increased by increasing the pinning site density and operating the detector at larger bias currents. The mechanisms of electron–vortex interaction, phonon–vortex interaction, and vortex dissipation have not been fully understood. Further investigation on the processing control and quantitative prediction of the sensitivity and response time will facilitate the realization of practical devices.

4. Thermal Modeling and Design

Thermal analysis is crucial for both thermal and nonequilibrium responses [14,25,63,64]. In the radiometric applications, thermal modeling can be employed to predict the error caused by the nonequivalence between the electrical heating and the radiative heating and to study the dynamic response [65].

Flik *et al.* [63] developed a detailed thermal model considering the radiation absorption in the

film–substrate composite and the boundary resistance between the film and the substrate. They compared their theoretical results with the measurements of Frenkel *et al.* [25]. The maximum temperature increase calculated from their model was 7 K for a 150 ps pulse with a substrate temperature of 50 K. This was more than three times larger than that calculated from a simple one-dimensional thermal conduction equation [25]. Although the bolometric effect predicted by the more sophisticated model was large, the results from [63] did not exclude the possible existence of nonbolometric response.

Fushinobu *et al.* [64] presented a three-dimensional numerical model for the microbolometer fabricated by Nahum *et al.* [23]. The calculated temperature change and phase lag depend strongly on the modulation frequency. They indicated that the approximate analysis employed by Hu and Richards [26] resulted in an error in the prediction of the thermal conductance. This error is small for modulation frequencies less than 1 kHz and could be as large as 25% at a modulation frequency of 30 kHz.

Zhang *et al.* [65] performed a thermal modeling of two absolute cryogenic radiometers using a finite element method. The radiometers measure the absolute radiant power using an electrical-substitution technique. One of the radiometers employed a superconducting kinetic-inductance thermometer as the sensing element [6]. The nonequivalence between the electrical and radiative heating was calculated to be less than 0.003% for this radiometer. The time constant was 11 s due to the large heat capacity of the conical receiver. It was shown that the time response could be improved by reducing the thickness of the black paint.

Neff [66] analyzed the effect of film thickness on the responsivity and *NEP* of superconducting bolometers. In his study, the dependence of absorptance on the film thickness was not considered. The film thickness, in fact, strongly influences the absorptance of the superconducting film–substrate composite [67,68]. Accurate determination of the thermophysical properties is essential for thermal modeling and design. The optical properties of high-T_c superconductors will be discussed in the next section, followed by a discussion on the thermal conductivity of superconducting films and boundary resistance between the film and the substrate.

4.1. Optical Properties

Knowledge of the optical constants of the detector materials is crucial for the radiative design of superconducting detectors. The optical constants can be extracted from the measured reflectance, transmittance, and absorptance. The two-fluid model is most frequently used in the far-infrared and microwave regions for both low-T_c and high-T_c superconductors, but it is not applicable for high-T_c superconductors in the mid-infrared [69]. The Mattis–Bardeen relations [70] are good for impure superconductors, where the electron mean free path is much shorter than the superconducting coherence length. The $YBa_2Cu_3O_7$ is a pure superconductor and, therefore, the Mattis–Bardeen relations do not apply [68,71]. Renk [72], Tanner and Timusk [73], and Timusk and Tanner [74] reviewed the theoretical and experimental studies of the optical properties of high-T_c superconductors.

Flik *et al.* [71] and Zhang *et al.* [75] proposed a method for the determination of the dielectric function of $YBa_2Cu_3O_7$ in the superconducting state. It accounts for the residual absorption by normal-state electrons, a finite electron scattering rate, and a mid-infrared absorption band due to interband electronic transitions. The dielectric function can be expressed by a linear superposition [74]:

$$\varepsilon(\omega) = \varepsilon_\infty + \varepsilon_{phonon} + \varepsilon_{mid\text{-}ir} + \frac{i\sigma(\omega)}{\varepsilon_0 \omega} \tag{16}$$

In the above equation, ε_∞ is the high-frequency dielectric constant, which is approximately equal to 4. The phonon contribution, ε_{phonon}, is negligible for the *a–b* plane of $YBa_2Cu_3O_7$ epitaxial films. The mid-infrared absorption band, $\varepsilon_{mid\text{-}ir}$, accounts for interband electronic transitions and is temperature-independent. The last term on the right is the free-carrier contribution, where ε_0 is the electrical permittivity of free space and $\sigma(\omega)$ is the free-carrier conductivity. The free-carrier conductivity term dominates the dielectric function in the infrared region. It is modeled using two components: the contribution of the electrons whose behavior can be described by the BCS theory [76], viz., BCS electrons that include both Cooper pairs and quasiparticles, and the contribution of the residual normal electrons (or holes) [75]:

$$\sigma(\omega) = (1 - f_{nr})\sigma_{ss}(\omega) + f_{nr}\sigma_{nr}(\omega) \tag{17}$$

where f_{nr} is the fraction of residual normal electrons, and σ_{ss} and σ_{nr} are the conductivities of BCS electrons and normal electrons, respectively. The complex conductivity of the BCS electrons is calculated using the algorithm developed by Zimmermann *et al.* [77]. The

input parameters are the electron scattering rate, β, the dc conductivity, $\sigma_0 = n_e e^2/(\beta m_e)$, where e, m_e, and n_e are the electron charge, effective mass, and number density, respectively, the temperature-dependent energy gap, $\Delta(T)$, and the ratio of the temperature of the superconducting films to the critical temperature, T/T_c. The conductivity of the residual normal electrons is calculated using the Drude free-electron model: $\sigma_{nr}(\omega) = \sigma_0/(1 - i\omega/\beta)$.

It was assumed that the electron scattering rate for both the BCS theory and the normal-state electrons is the same. Equation (17) is used to account for the residual absorption and, therefore, the fraction of residual normal electrons does not depend on temperature. It should not be confused with the conventional two-fluid model for the optical conductivity, where the fraction of normal-state electrons depends on temperature.

Figure 9 compares the reflectivity calculated from the proposed dielectric function, Eq. (16), to six sets of data obtained by different research groups, two for single crystals [78, 79] and four for epitaxial films [80–83]. The agreement suggests that the dielectric function model is suitable for engineering applications, although there are no conclusive solutions right now regarding the electron–phonon coupling mechanism, the energy gap, and the origin of the residual absorption in the high-T_c superconductors [75].

Figure 10 shows the absorptance of $YBa_2Cu_3O_7$ on $LaAlO_3$ at 78 K. The absorptance is calculated by subtracting the reflectance obtained in [71] from unity since the substrate is opaque in the spectral region from 10 to 100 μm. Without a proper design, a high-T_c superconducting infrared detector using the film–substrate composite as the absorber may not be a broadband detector because the absorptance is a strong function of the wavelength of the incident radiation. The absorptance in the wavelength regions from 10 to 13 μm, 25 to 34 μm, and 60 to 100 μm strongly increases with decreasing film thickness. This implies that the responsivity of an infrared detector can be increased by reducing the film thickness. The effect of oxygen stoichiometry on the optical properties of $YBa_2Cu_3O_{7-\delta}$ films was investigated by Choi *et al.* [84]. They found a strong dependence of the optical constants on the oxygen content.

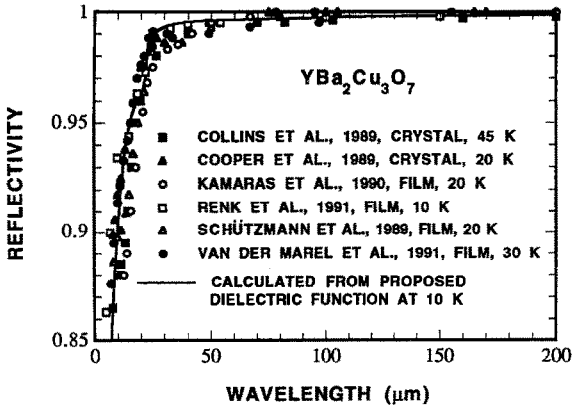

Fig. 9. Comparison of the reflectivity of $YBa_2Cu_3O_7$ calculated from the proposed dielectric function, Eq. (16), to six sets of data (from [75]).

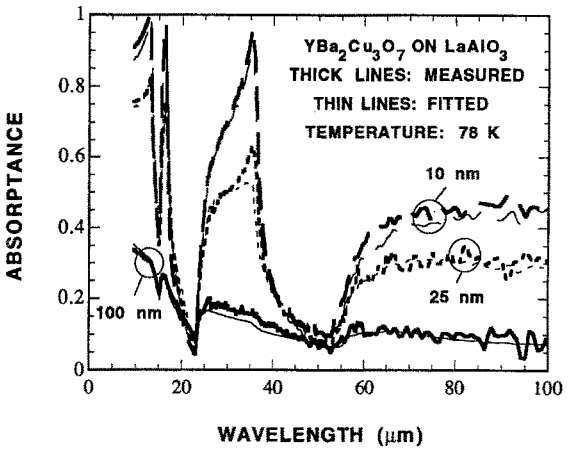

Fig. 10. Absorptance of $YBa_2Cu_3O_7$ on $LaAlO_3$ at 78 K for different film thicknesses calculated from the reflectance obtained by Flik *et al.* [71].

For the $YBa_2Cu_3O_7$ films on silicon substrates, optimization of the detector design requires the determination of the absorptance of $YBa_2Cu_3O_7$/YSZ/Si multilayer structures. Zhang and Flik [85] presented an algorithm for calculating the absorptance of multilayer structures. Using the method described in [85], the absorptance is calculated for radiation incident either on the $YBa_2Cu_3O_7$ film side or on the silicon side. The transmittance is the same while the reflectance for irradiation from the silicon side is less than that for irradiation from the film side. Hence, the absorptance improves if the radiation is incident on the Si substrate. Figure 11 shows the absorptance calculated for different film thicknesses at 78 K for radiation incident on the Si substrate. As film thickness increases, the transmittance decreases while the reflectance increases. The competing effects yield an optimized film thickness for largest absorptance at a given wavelength. The absorption at wavelengths less than 1.12 μm, the band gap of silicon, is due to the fundamental absorption of silicon. The absorption peaks in the mid-infrared region are due to the

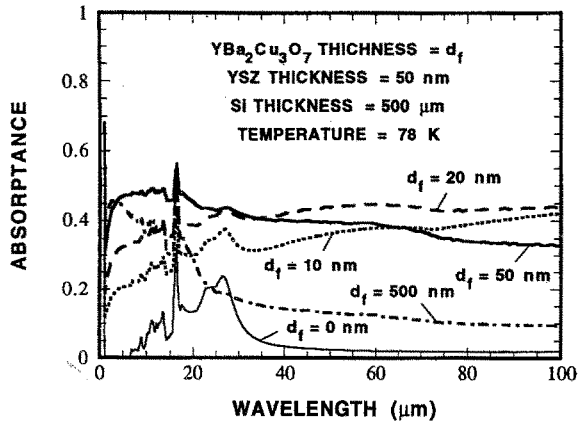

Fig. 11. Predicted absorptance of $YBa_2Cu_3O_7$/YSZ/Si multilayer structures at 78 K, where the radiation is incident from the backside, i.e., on the Si substrate.

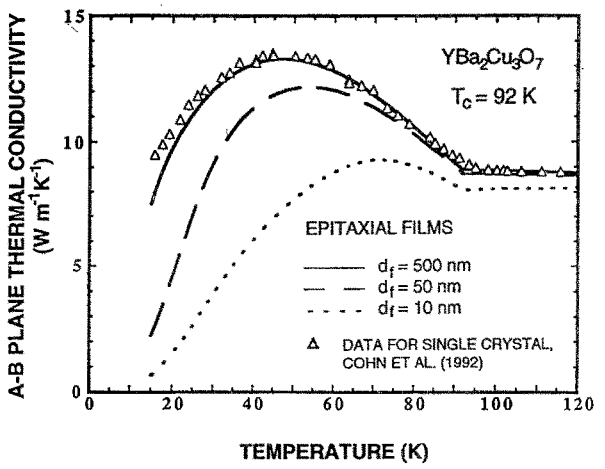

Fig. 12. Thermal conductivity of the a–b plane $YBa_2Cu_3O_7$ (from [91] by permission of the author).

phonon and impurity absorption of silicon and YSZ. Films with thickness of 20 nm exhibit the highest absorptance of approximately 0.40 for wavelengths between 1 and 100 μm. The above calculation is based on the optical constants obtained for $YBa_2Cu_3O_7$ films deposited on $LaAlO_3$ substrates [71]. The effects of film thickness and microstructure on the optical constants of $YBa_2Cu_3O_7$ and YSZ films deposited on silicon substrates should be investigated experimentally.

4.2. Thermal Conductivity and Boundary Resistance

Measurement of the thermal conductivity of high-T_c superconductors was reviewed by Flik [86] and Uher [87,88]. The anisotropy of the thermal conductivity for bulk high-T_c superconductors is due to their anisotropic crystalline structures. The size effect on the thermal conductivity of high-T_c superconducting films due to boundary scattering was investigated by Flik and Tien [89], Richardson *et al.* [90], and Goodson and Flik [91]. At temperatures near 100 K, about 30% of the thermal conductivity is due to electrons [90]. Goodson and Flik [91] showed that, in the a–b plane of the $YBa_2Cu_3O_7$ below 60 K where the size effect in the films is significant, the thermal conductivity due to phonons is much larger than that due to electrons. Figure 12 shows the a–b plane thermal conductivity of the $YBa_2Cu_3O_7$, where the predicted thermal conductivity for thin films is compared to the data of a single crystal reported in [92]. The value of the thermal conductivity for a given film depends on the particular defect structure [90]. The anisotropy of the thermal conductivity of c-axis-oriented $YBa_2Cu_3O_7$ films was investigated by Shaw-Klein *et al.* [93] at room temperature. The reduction for both the a–b plane and c-axis thermal conductivities was attributed to the microstructure. Challenges remain in the experimental determination of the thermal conductivity of high-T_c superconducting thin films at cryogenic temperatures.

Thermal boundary resistance between the film and the substrate strongly affects the performance of the superconducting detector. As discussed in Section 2.1, a fast bolometric response could be made possible by optimizing the boundary resistance between the film and the substrate. The boundary resistance, R_{bd}, obtained by different groups [10,94–96], between $YBa_2Cu_3O_7$ and MgO, sapphire, or $LaAlO_3$ and that between Tl–Ba–Ca–Cu–O and MgO, showed consistently a value approximately 10^{-7} K m^2 W^{-1} at temperatures from 80 to 300 K. This is about two orders of magnitude larger than that predicted by the acoustic mismatch theory [97]. The dominant phonon wavelength for heat conduction decreases with temperature. At temperatures larger than 30 K, the dominant phonon wavelength is less than 1 nm [98], which is comparable with the mean roughness of the film–substrate interface. The assumption of a perfect interface made in the acoustic mismatch theory may break down. Phelan *et al.* [98] directly measured the boundary resistance between an Er–Ba–Cu–O film and a MgO substrate using a technique described by Swartz and Pohl [99]. They obtained a boundary resistance of larger than 10^{-5} K m^2 W^{-1} at temperatures from 64 to 137 K.

As suggested in [11], by introducing $PrBa_2Cu_3O_7/LaAlO_3$ between the $YBa_2Cu_3O_7$ film

and the substrate, an increase of the bolometric responsivity could be obtained with longer pulse duration. On the other hand, by eliminating the boundary resistance using the structure proposed in [14], sensitive nonequilibrium response could be realized on a picosecond time scale. Further research is needed to study the origin of the large boundary resistance and the effects of the substrate surface treatment and film deposition conditions on the boundary resistance.

4.3. Refrigeration and Temperature Control

Cryogenic refrigeration is required to achieve the operating temperature of the superconducting detectors. Cooling techniques include the use of cryogen, mechanical or thermoelectric refrigeration, and radiation cooling in space applications. Various types of cryogenic coolers suitable for infrared systems were reviewed by Breckenridge [100]. Although liquid helium and nitrogen can be used in research laboratories, it is preferred to use closed-cycle refrigerating systems in many applications. The use of high-T_c superconductors eases the requirement for cooling down to very low temperatures. There are research opportunities for closed-cycle cooling in the region between 40 and 90 K [101]. It is important to improve the reliability and efficiency of these systems.

Another issue is temperature control and stability. For bolometric applications, the temperature of the superconducting bridge must be controlled precisely in the transition region. The transition width of high-quality films is less than a kelvin. Thermal fluctuations limit the sensitivity and accuracy of absolute radiometers [65]. For the highly sensitive and accurate radiometric application, temperature stability of the order of a microkelvin or better is required. Further studies are needed to improve the temperature control system.

5. SUMMARY AND FUTURE RESEARCH

Both fast and slow bolometric responses exist in superconductors. The former, occurring on a time scale from 1 ns to 10 μs, may be attributed to the heating of the superconducting film relative to the substrate. The latter, occurring on a time scale from 10 μs to 1 s depending on the particular structure, is attributed to the heating of both the film and the substrate relative to the heat sink.

The potential of high-T_c superconducting microbolometers and detector arrays fabricated on silicon and silicon nitride membranes has been demonstrated. It is foreseeable that these devices will outperform other detectors operating at or above 77 K due to their broadband spectral sensitivity, low cost, and silicon compatibility. System issues such as detector and array uniformity, integrated read-out electronics, contact noise, thermal stability, etc., must be further investigated.

The distinction between the nonequilibrium response and the thermal response lies in (1) that nonequilibrium response happens at temperatures below T_c and is not proportional to dR/dT and (2) that nonequilibrium response can happen in a very short time, from less than a nanosecond down to picoseconds. A photoresponse time of approximately 20 ps has been observed for high-T_c superconducting films. The mechanisms of quasiparticle–vortex interaction, phonon–vortex interaction, and vortex dissipation should be investigated. Quantitative predictions of the responsivity and response time are required for practical applications.

Thermal modeling and design are very important for the understanding of the photoresponse mechanism and for the construction of superconducting radiation detectors. Experiments are needed to determine the effects of microstructure and film thickness on the thermophysical properties of thin films.

Further improvement of the cooling and temperature control techniques will expedite the future development of high-T_c superconducting radiation detectors.

ACKNOWLEDGMENTS

The authors would like to thank Dr. R. U. Datla, Dr. C. W. Clark, and Dr. R. A. MacDonald of NIST and Professor H. D. Drew of the University of Maryland for valuable discussions and comments. Z.M.Z. is grateful to his doctoral advisor, Professor M. I. Flik, for leading him to the areas of microscale heat transfer and superconductivity and for continuous encouragement.

REFERENCES

1. P. L. Richards, J. Clarke, R. Leoni, Ph. Lerch, S. Verghese, M. R. Beasley, T. H. Geballe, R. H. Hammond, P. Rosenthal and S. R. Spielman, *Appl. Phys. Lett.* **54**, 283 (1989).
2. J. Clarke, G. I. Hoffer, P. L. Richards and N.-H. Yeh, *J. Appl. Phys.* **48**, 4865 (1977).
3. P. W. Kruse, *Semicond. Sci. Technol.* **5**, S229 (1990).
4. A. Frenkel, *Physica C* **180**, 251 (1991).
5. I. A. Khrebtov, *Sov. J. Opt. Technol.* **58**, 261 (1991).

6. J. E. Sauvageau, D. G. McDonald and E. N. Grossman, *IEEE Trans. Magn.* **27**, 2757 (1991).
7. D. G. McDonald, *Appl. Phys. Lett.* **50**, 775 (1987).
8. J. Brasunas, B. Lakew and C. Lee, *J. Appl. Phys.* **71**, 3639 (1992).
9. M. I. Flik, Z. M. Zhang and K. E. Goodson, *Appl. Phys. Lett.* **62**, 2862 (1993).
10. G. L. Carr, M. Quijada, D. B. Tanner, C. J. Hirschmugl, G. P. Williams, S. Etemad, B. Dutta, F. DeRosa, A. Inam, T. Venkatesan and X. Xi, *Appl. Phys. Lett.* **57**, 2725 (1990).
11. C. G. Levey, S. Etemad and A. Inam, *Appl. Phys. Lett.* **60**, 126 (1992).
12. S. Verghese, P. L. Richards, K. Char, D. K. Fork and T. H. Geballe, *J. Appl. Phys.* **71**, 2491 (1992).
13. B. R. Johnson, T. Ohnstein, C. J. Han, R. Higashi, P. W. Kruse, R. A. Wood, H. Marsh and S. B. Dunham, *IEEE Trans. Appl. Supercond.* **3**, 2856 (1993).
14. A. Frenkel, *Phys. Rev. B* **48**, 9717 (1993).
15. R. A. Smith, F. E. Jones and R. P. Chasmar, *The Detection and Measurement of Infra-Red Radiation*, 2nd edn. (Oxford University Press, London, 1968).
16. V. L. Newhouse, *Applied Superconductivity* (Wiley, New York, 1964), Chap. 8.
17. F. J. Low and A. R. Hoffman, *Appl. Opt.* **2**, 649 (1963).
18. R. C. Jones, *Proc. IRE* **47**, 1481 (1959).
19. P. Rosenthal, R. H. Hammond, M. R. Beasley, R. Leoni, Ph. Lerch and J. Clarke, *IEEE Trans. Magn.* **25**, 973 (1989).
20. J. Brasunas and B. Lakew, *Proc. SPIE* **1477**, 166 (1991).
21. S. Verghese, P. L. Richards, K. Char and S. A. Sachtjen, *IEEE Trans. Magn.* **27**, 3077 (1991).
22. M. Lindgren, H. Ahlberg, A. Larsson, S. T. Eng and M. Danerud, *Phys. Scr.* **44**, 105 (1991).
23. M. Nahum, Q. Hu, P. L. Richards, S. A. Sachtjen, N. Newman and B. F. Cole, *IEEE Trans. Magn.* **27**, 3081 (1991).
24. B. Dwir and D. Pavuna, *J. Appl. Phys.* **72**, 3855 (1992).
25. A. Frenkel, M. A. Saifi, T. Venkatesan, P. England, X. D. Wu and A. Inam, *J. Appl. Phys.* **67**, 3054 (1990).
26. Q. Hu and P. L. Richards, *Appl. Phys. Lett.* **55**, 2444 (1989).
27. K. Li, J. E. Johnson and B. W. Aker, *J. Appl. Phys.* **73**, 1531 (1993).
28. T. G. Stratton, B. E. Cole, P. W. Kruse, R. A. Wood, K. Beauchamp, T. F. Wang, B. Johnson and A. M. Goldman, *Appl. Phys. Lett.* **57**, 99 (1990).
29. D. B. Fenner, Q. Li, W. D. Hamblen, M. E. Johansson, D. G. Hamblen, L. Lynds and J. I. Budnick, *IEEE Trans. Appl. Supercond.* **3**, 2104 (1993).
30. Q. Li, D. B. Fenner, W. D. Hamblen, and D. G. Hamblen, *Appl. Phys. Lett.* **62**, 2428 (1993).
31. C. A. Bang, M. I. Flik, M. A. Schmidt and Z. M. Zhang, United States Patent No. 5264375 (1993).
32. C. A. Bang, J. P. Rice, M. I. Flik, D. A. Rudman and M. A. Schmidt, *J. Microelectromech. Syst.* **2**, 160 (1993).
33. T. P. Orlando and K. A. Delin, *Foundations of Applied Superconductivity* (Addison-Wesley, Reading, Massachusetts, 1991), Chap. 3.
34. B. I. Verkin, B. B. Banduryan, A. V. Bondarenko, V. G. Efremenko, V. A. Konovodchenko, M. A. Obolenskii and G. V. Shustakova, *Sov. J. Low Temp. Phys.* **14**, 387 (1988).
35. D. Robbes, P. Langlois, C. Dolabdjian, D. Bloyet, J. F. Hamet and H. Murray, *IEEE Trans. Appl. Supercond.* **3**, 2123 (1993).
36. A. Gilabert, *Ann. Phys. Fr.* **15**, 255 (1990).
37. K. E. Gray, ed., *Nonequilibrium Superconductivity, Phonons, and Kapitza Boundaries* (Plenum Press, New York, 1981).
38. D. N. Langenberg and A. I. Larkin, eds., *Nonequilibrium Superconductivity* (North-Holland, Amsterdam, Holland, 1986).
39. J. A. Pals, K. Weiss, P. M. T. M. van Attekum, R. E. Horstman, and J. Wolter, *Phys. Rep.* (review section of *Phys. Lett.*) **89**, 323 (1982).
40. Y. Enomoto and T. Murakami, *J. Appl. Phys.* **59**, 3807 (1986).
41. T. Nishino, H. Nakane, Y. Tarutani, M. Hirano, T. Aida, S. Kominami, and U. Kawabe, *Jpn. J. Appl. Phys.* **26**, L1320 (1987).
42. J. C. Culbertson, U. Strom, S. A. Wolf and W. W. Fuller, *Phys. Rev. B* **44**, 9609 (1991).
43. M. Leung, U. Strom, J. C. Culbertson, J. H. Claassen, S. A. Wolf and R. W. Simon, *Appl. Phys. Lett.* **50**, 1961 (1987).
44. D. P. Osterman, P. Marr, H. Dang, C.-T. Yao and M. Radparvar, *IEEE Trans. Magn.* **27**, 2681 (1991).
45. D. P. Osterman, R. Patt and R. Madhavrao, *IEEE Trans. Appl. Supercond.* **3**, 2860 (1993).
46. H. S. Kwok, J. P. Zheng, Q. Y. Ying and R. Rao, *Appl. Phys. Lett.* **54**, 2473 (1989).
47. E. Zeldov, N. M. Amer, G. Koren and A. Gupta, *Phys. Rev. B* **39**, 9712 (1989).
48. A. Frenkel, M. A. Saifi, T. Venkatesan, C. Lin, X. D. Wu, and A. Inam, *Appl. Phys. Lett.* **54**, 1594 (1989).
49. M. Johnson, *Appl. Phys. Lett.* **59**, 1371 (1991).
50. A. D. Semenov, G. N. Gol'tsman, I. G. Gogidze, A. V. Sergeev, P. T. Lang and K. F. Renk, *Appl. Phys. Lett.* **60**, 903 (1992).
51. R. S. Nebosis, R. Steinke, P. T. Lang, W. Schatz, M. A. Heusinger, K. F. Renk, G. N. Gol'tsman, B. S. Karasik, A. D. Semenov, and E. M. Gershenzon, *J. Appl. Phys.* **72**, 5496 (1992).
52. A. Ghis, J. C. Villegier, S. Pfister, M. Nail and Ph. Gibert, *Appl. Phys. Lett.* **63**, 551 (1993).
53. N. Bluzer, *Phys. Rev. B* **44**, 10222 (1991).
54. N. Bluzer, *J. Appl. Phys.* **71**, 1336 (1992).
55. S. G. Han, Z. V. Vardeny, K. S. Wong, O. G. Symko and G. Koren, *Phys. Rev. Lett.* **65**, 2708 (1990).
56. S. D. Brorson, A. Kazeroonian, D. W. Face, T. K. Cheng, G. L. Doll, M. S. Dresselhaus, G. Dresselhaus, E. P. Ippen, T. Venkatesan, X. D. Wu and A. Inam, *Solid State Commun.* **74**, 1305 (1990).
57. J. M. Chwalek, C. Uher, J. F. Whitaker, G. A. Mourou, J. Agostinelli and M. Lelental, *Appl. Phys. Lett.* **57**, 1696 (1990).
58. E. N. Grossman, D. G. McDonald and J. E. Sauvageau, *IEEE Trans. Magn.* **27**, 2677 (1991).
59. S. I. Anisimov, B. L. Kapeliovich, and T. L. Perel'man, *Sov. Phys. JETP* **39**, 375 (1974).
60. T. Q. Qiu and C. L. Tien, *Int. J. Heat Mass Transfer* **35**, 719 (1992).
61. A. Rothwarf and B. N. Taylor, *Phys. Rev. Lett.* **19**, 27 (1967).
62. C. S. Owen and D. J. Scalapino, *Phys. Rev. Lett.* **28**, 1559 (1972).
63. M. I. Flik, P. E. Phelan, and C. L. Tien, *Cryogenics* **30**, 1118 (1990).
64. K. Fushinobu, P. E. Phelan, K. Hijikata, T. Nagasaki and M. I. Flik, *J. Heat Transfer* **116**, 275 (1994).
65. Z. M. Zhang, R. U. Datla, S. R. Lorentz and H. C. Tang, to appear in *J. Heat Transfer* (November, 1994).
66. H. Neff, *J. Appl. Phys.* **69**, 8375 (1991).
67. P. E. Phelan, G. Chen and C. L. Tien, *J. Heat Transfer* **114**, 227 (1992).
68. Z. M. Zhang, B. I. Choi, T. A. Le, M. I. Flik, M. P. Siegal and J.M. Philips, *J. Heat Transfer* **114**, 644 (1992).
69. P. E. Phelan, M. I. Flik and C. L. Tien, *J. Heat Transfer* **113**, 487 (1991).
70. D. C. Mattis and J. Bardeen, *Phys. Rev.* **111**, 412 (1958).
71. M. I. Flik, Z. M. Zhang, K. E. Goodson, M. P. Siegal and J. M. Phillips, *Phys. Rev. B* **46**, 5606 (1992).
72. K. F. Renk, in *Studies of High-Temperature Superconductors*, A. V. Narlikar, ed., Vol. 10 (Nova Science Publishers, New York, 1992).
73. D. B. Tanner and T. Timusk, in *Physical Properties of High-Temperature Superconductors*, D. M. Ginsberg, ed., Vol. 3 (World Scientific, Singapore, 1992), pp. 363–469.

74. T. Timusk and D. B. Tanner, in *Physical Properties of High-Temperature Superconductors*, D. M. Ginsberg, ed., Vol. 1 (World Scientific, Singapore, 1989), pp. 339–407.
75. Z. M. Zhang, T. A. Le, M. I. Flik and E. G. Cravalho, *J. Heat Transfer* **116**, 253 (1994).
76. J. Bardeen, L. N. Cooper and J. R. Schrieffer, *Phys. Rev.* **108**, 1175 (1957).
77. W. Zimmermann, E. H. Brandt, M. Bauer, E. Seider and L. Genzel, *Physica C* **183**, 99 (1991).
78. R. T. Collins, Z. Schlesinger, F. Holtzberg and C. Feild, *Phys. Rev. Lett.* **63**, 422 (1989).
79. S. L. Cooper, G. A. Thomas, J. Orenstein, D. H. Rapkine, M. Capizzi, T. Timusk, A. J. Millis, L. F. Schneemeyer and J. V. Waszczak, *Phys. Rev. B.* **40**, 11358 (1989).
80. K. Kamaras, S. L. Herr, C. D. Porter, N. Tache, D. B. Tanner, S. Etemad, T. Venkatesan, E. Chase, A. Inam, X. D. Wu, M. S. Hegde and B. Dutta, *Phys. Rev. Lett.* **64**, 84 (1990).
81. K. F. Renk, B. Gorshunov, J. Schützmann, A. Prückl, B. Brunner, J. Betz, S. Orbach, N. Klein, G. Müller and H. Piel, *Europhys. Lett.* **15** 661 (1991).
82. J. Schützmann, W. Ose, J. Keller, K. F. Renk, B. Roas, L. Schultz and G. Saemann-Ischenko, *Europhys. Lett.* **8**, 679 (1989).
83. D. van der Marel, H.-U. Habermeier, D. Heitmann, W. König and A. Wittlin, *Physica C* **176**, 1 (1991).
84. B. I. Choi, Z. M. Zhang, M. I. Flik and T. Siegrist, *J. Heat Transfer* **114**, 958 (1992).
85. Z. M. Zhang and M. I. Flik, *IEEE Trans. Appl. Supercond.* **3**, 1604 (1993).
86. M. I. Flik, *Appl. Mech. Rev.* **44**, 93 (1991).
87. C. Uher, *J. Supercond.* **3**, 337 (1990).
88. C. Uher, in *Physical Properties of High-Temperature Superconductors*, D. M. Ginsberg, ed., Vol. 3 (World Scientific, Singapore, 1992), pp. 159–284.
89. M. I. Flik and C. L. Tien, *J. Heat Transfer* **112**, 872 (1990).
90. R. A. Richardson, S. D. Peacor, C. Uher and F. Nori, *J. Appl. Phys.* **72**, 4788 (1992).
91. K. E. Goodson and M. I. Flik, *J. Heat Transfer* **115**, 17 (1993).
92. J. L. Cohn, S. A. Wolf, T. A. Vanderah, V. Selvamanickam and K. Salama, *Physica C* **192**, 435 (1992).
93. L. J. Shaw-Klein, S. J. Burns, A. M. Kadin, S. D. Jacobs and D. S. Mallory, *Supercond. Sci. Technol.* **5**, 368 (1992).
94. M. Nahum, S. Verghese, P. L. Richards and K. Char, *Appl. Phys. Lett.* **59**, 2034 (1991).
95. C. D. Marshall, I. M. Fishman and M. D. Fayer, *Phys. Rev. B* **43**, 2692 (1991).
96. S. Zeuner, H. Lengfellner, J. Betz, K. F. Renk and W. Prettl, *Appl. Phys. Lett.* **61**, 973 (1992).
97. W. A. Little, *Can. J. Phys.* **37**, 334 (1959).
98. P. E. Phelan, O. Nakabeppu, K. Ito, K. Hijikata and T. Ohmori, in *Heat Transfer in Superconducting Equipment*, P. W. Eckels and K. M. Obasih eds., ASME HTD Vol. 229 (ASME, New York, 1992), pp. 33–38.
99. E. T. Swartz and R. O. Pohl, *Rev. Mod. Phys.* **61**, 605 (1989).
100. R. W. Breckenridge, Jr., *Opt. Eng.* **14**, 57 (1975).
101. D. K. Christen, R. C. Dynes, V. J. Emery, C. M. Falco, D. U. Gubser, S. Jin, H. Kroger and D. T. Shaw, *Cryogenics* **32**, 338 (1992).